Hydrogen uptake and optical properties of sputtered Mg–Ni thin films

2004 J. Phys.: Condens. Matter 16 7649

(http://iopscience.iop.org/0953-8984/16/43/008)

INSTITUTE OF PHYSICS PUBLISHING JOURNAL OF PHYSICS: CONDENSED MATTER

J. Phys.: Condens. Matter **16** (2004) 7649–7662 PII: S0953-8984(04)83570-7

Hydrogen uptake and optical properties of sputtered Mg–Ni thin films

Emil Johansson[1], Cyril Chacon[1], Claudia Zlotea[2], Yvonne Andersson[2] and Björgvin Hjörvarsson[1,3]

[1] Department of Physics, Uppsala University, Box 530, S-751 21, Uppsala, Sweden
[2] Department of Materials Chemistry, Uppsala University, Box 538, S-751 21, Uppsala, Sweden

E-mail: bjorgvin.hjorvarsson@fysik.uu.se

Received 11 July 2004
Published 15 October 2004
Online at stacks.iop.org/JPhysCM/16/7649
doi:10.1088/0953-8984/16/43/008

Abstract

The hydrogen uptake and distribution in wedged Mg–Ni films, with composition ranging from $Mg_{0.85}Ni_{0.15}$ to $Mg_{0.55}Ni_{0.45}$, were investigated. Upon hydrogen loading at 298 K these films undergo a transition from a mirror-like metallic to a semiconducting transparent state. After exposure to a hydrogen pressure of 1 bar, the samples exhibit large variation in optical appearance, ranging from a pale yellowish (Mg rich side) to a brownish shade (Ni rich side). The change in the effective optical band gap E_g^{eff} as a function of sample composition and hydrogen concentration was determined; it showed changes from 3.6 eV in the Ni poor domain to 2.4 eV in the Ni rich domain. Composition analysis using the ^{15}N nuclear resonance method showed close to homogeneous hydrogen distribution throughout the film and close to linear increase in the hydrogen uptake with increasing Mg content. The thermal stability of the films is limited; annealing above 393 K results in significant redistribution of the constituents. Mg is enriched at the surface, reacting with Pd and thereby degrading the capping layer through the formation of Mg_6Pd and MgO, as determined by x-ray diffraction, x-ray photoelectron spectroscopy and Rutherford backscattering studies. This redistribution results in a severe decrease of the hydrogen uptake rate, as monitored by *in situ* resistivity measurements.

(Some figures in this article are in colour only in the electronic version)

1. Introduction

Mg reacts with hydrogen and forms MgH_2 which yields a maximum hydrogen storage capacity of 7.6 wt%. Although the storage capacity of Mg is large, the use of Mg as a storage medium

[3] Author to whom any correspondence should be addressed.

is hampered by thermodynamic and kinetic limitations [1]. The absorption and desorption temperatures are too high; this is partially caused by the low diffusion rate of H in the MgH_2 β-phase [2]. Alloying Mg with elements that do not form stable hydrides, such as Ni, can significantly improve the thermodynamic and kinetic properties. In 1968 Reilly *et al* [3] discovered the hydrogen absorbing capabilities of Mg_2Ni. This material combination has been extensively studied, mainly through various bulk techniques [4, 5]. The intermetallic compound Mg_2Ni absorbs hydrogen, initially forming $Mg_2NiH_{0.3}$ without any structural rearrangement and, upon further hydrogen loading, Mg_2NiH_4 is formed corresponding to 3.6 wt% of hydrogen [3]. The hydrogen storage capacity is reduced, as compared to pure Mg, but the thermodynamic and kinetic properties are significantly improved, i.e. lower absorption and desorption temperatures are obtained [6].

The results on the hydrogen uptake of Mg–Ni alloys prepared by traditional casting methods scatter significantly. By using thin film synthesis techniques such as sputtering, it is possible to overcome some of the problems and at the same time to distinguish between the limitations imposed by the bulk and surface properties. The use of thin films as model systems for investigating hydrogen storage capabilities is rare. Holtz *et al* [7, 8] deposited Mg–Ni alloys by co-sputtering of Mg and Ni. The films were scraped off the substrate and pressed into pellets with Ni ratios of 15, 33 and 60 at.%. The hydrogen uptake capacities for the different compositions were deduced to be approximately 5, 4 and 2 wt% respectively. To achieve the maximum uptake, the samples had to be hydrided for times of approximately 35, 50 and 15 h respectively, illustrating the improvement of the kinetics with increasing Ni content. The films disintegrated and fragmented into fine powder upon hydrogen loading, with a hydrogen uptake close to the theoretical maximum of Mg_2NiH_4. Chen *et al* [9] prepared amorphous Mg–Ni films using ion-beam sputtering and investigated the hydriding and dehydriding properties by means of DSC (differential scanning calorimetry) and XRD (x-ray diffraction) measurements. On the basis of the DSC measurements they deduced ΔH_{abs} to be -39.8 kJ mol^{-1} H_2 and ΔH_{des} to be 42 kJ mol^{-1} H_2 in a $Mg_{1.2}Ni_{1.0}H$ film. The heat of formation is smaller than that obtained theoretically for bulk Mg_2NiH_4 (approximately 64 kJ mol^{-1}), implying weaker M–H bonding in the amorphous film as compared to crystalline Mg_2NiH_4 [9].

The absorption of H implies large changes in the electronic structure of Mg. The hydride (α-MgH_2) is non-metallic and transparent and the band gap has been deduced to be in the range of 3.1–4.2 eV through various theoretical calculations (see for example [10] and references therein). The few existing experimental values are substantially higher; for example, Isidorsson *et al* determined E_g for α-MgH_2 with the Rayleigh as well as the Lambert–Beer formalism and their result implied a level of E_g between 5.61 and 5.67 eV [10]. The Mg–Ni system is not only interesting from a hydrogen storage point of view; Mg_2NiH_4 films have been reported to behave as switchable mirrors. Upon hydrogen loading these films change from a shiny reflecting metallic to a transparent semiconducting state [11–14]. E_g for Mg_2NiH_4 is determined as approximately 1.6 eV [11, 12, 15]. Therefore Mg thin films alloyed with Ni can be used as a model system for studying the impact of added d elements on the electronic structure of Mg based alloys.

The reactivity of Mg with oxygen and water is well documented and the influence of the presence of oxides and hydroxides must therefore be considered in the current context. The optical band gap of MgO is 7.77 eV [16], which is substantially higher than that for MgH_2. The presence of oxides can therefore result in an overestimation of the optical band gap of the hydride. Special care has therefore to be taken regarding the chemical purity of the samples.

In this paper, two different routes for synthesizing Mg–Ni films by DC magnetron sputtering will be discussed. Initially the possibility of forming Mg–Ni alloys through thermally activated diffusion of nanometre thick layers, called annealing in the coming sections,

will be addressed. Thereafter we discuss the growth of wedged multilayers, where the thickness of the individual layers is on the monolayer scale. The use of extremely thin layers allows direct production of the alloys through controlled intermixing during the growth process, which eliminates the need for post-annealing. Furthermore, the use of wedged structures allows the growth of samples where the composition varies linearly with position. Finally, the hydrogen uptake and the changes in the optical properties with composition will be addressed.

2. Experimental details

2.1. Sample preparation

The Mg–Ni samples were prepared using a custom designed ultrahigh vacuum (UHV) DC magnetron sputtering system with three targets, Mg, Ni and Pd. The purities of the target materials were 99.95%, 99.999% and 99.995% respectively. A pneumatic shutter controls the Mg flux while a motorized shutter is situated in front of the Ni target enabling the growth of Ni wedges. The main chamber is pumped by a turbomolecular pump (TMP) supported by a diaphragm fore-vacuum pump giving a base pressure typically in the 10^{-13} bar region. Residual gases were monitored by a quadrupole mass spectrometer. The load lock is evacuated using a TMP with a rotary vane fore-vacuum pump. The substrates (Corning 7059 glass and polished pyrolytic graphite) were solvent cleaned *ex situ* and baked *in situ* at 500 K for 10 h prior to sample growth. The sputtering gas (Ar, 99.9999% purity) was additionally purified using a West Associates ULTRAPURE gas purifier and the sputtering gas pressure was monitored and controlled by a Balzers-Leybold capacitance manometer (0–1.33×10^{-4} bar full scale) connected to a Granville-Philips 216 servo-driven leak valve. The magnetron discharges were generated by a DC power of 20 W (constant power mode) at an Ar pressure of 3.3×10^{-6} bar giving deposition rates of 0.019 and 0.059 nm s^{-1} for Mg and Ni respectively. The deposition rates were determined by x-ray reflectivity measurements using a Philips PW 3020 with Cu Kα radiation on single films of the pure elements. The substrates were held at a floating potential and prior to any deposition the targets were pre-sputtered for 15 min.

Two different types of sample were synthesized, with and without a wedge. Both were grown on 0.5 cm $\times$ 1 cm substrates. The samples with constant repeat distance equal to 2 nm were grown with thickness ratios of Mg and Ni equal to $1/4$, $1/2$ and $3/4$. The resulting total thickness is set to be 100 nm. The films were capped by a 10 nm Pd layer serving both as a catalyst for hydrogen dissociation and an oxidation barrier [17]. The wedge samples were grown with 200 repetitions with a bilayer thickness of 0.3 nm (Ni—0.2 to 0 nm and Mg—0.1 nm) at one end of the sample and with a Ni thickness of close to zero at the other end, resulting in approximately 60 and 40 nm total thickness at the each end for the films. These films were also covered by a 10 nm Pd capping layer.

2.2. Post-annealing and hydrogen loading

The post-annealing and the hydrogen loading were accomplished in the same set-up. The experimental set-up has been extensively described before—see, for example, Stillesjö *et al* [18]—and therefore only a brief description will be given here. The temperature was controlled and monitored by a Eurotherm 2408 temperature controller using a type K (chromel–alumel) thermocouple with an accuracy of 0.1 K. The four-probe resistivity measurements were accomplished using a combination of a Keithley 2400 source-meter and Keithley 2182 nanovoltmeter. The hydrogen gas, of 99.9996% purity, was additionally purified in two steps: initially by a West Associates ULTRAPURE gas purifier and thereafter by

absorption/desorption in a metal hydride storage bed. Prior to any measurement, the complete system, including the sample holder, was evacuated to a pressure below 10^{-11} bar. While pumping, the main contribution to the residual gas, as determined by the quadrupole mass spectrometer, is hydrogen. Pressure reading was performed using one of three capacitance manometers (0–1.33×10^{-3}, 0–0.133 and 0–1 bar full scale) depending on the applied hydrogen pressure.

The wedged multilayered samples were slowly loaded with hydrogen. Initially the samples were exposed to a hydrogen pressure of 5×10^{-4} bar at 298 K and after approximately 2–3 min the system was evacuated. This procedure was repeated four times in order to remove or dilute any oxygen containing species on the surface that might degrade the uptake. Thereafter a pressure of 10^{-3} bar was applied and when equilibrium was obtained, as determined from the resistivity measurements, the pressure was increased. The pressure was increased in steps up to the maximum applied pressure of 1 bar. The fully loaded state corresponds to an exposure of the sample to 1 bar for several days.

2.3. Sample characterization

High angle θ–2θ ($2\theta = 10°$–$90°$) XRD measurements were performed with a Bruker D5000 equipped with a graphite monochromator and divergence, anti-scatter and Soller slits. XRD measurements were performed before and after annealing with the objective of establishing an understanding of some of the changes caused by the annealing. XPS depth profiling (x-ray photoelectron spectroscopy) and RBS (Rutherford backscattering) were used to establish information about the chemical composition as well as gradients in the samples. The XPS measurements were performed using a Phi Quantum 2000 x-ray photoelectron spectrometer with a monochromatic Al Kα source of 1486.6 eV for a total of 16 points equally distributed along two parallel lines on the sample. The total sputtering time for the depth profile was approximately 12 min with a total of 14 cycles—in intervals of 6 s for the first eight cycles, 1 min for the next five cycles and 3 min for the last two cycles. As shown in figure 2, the substrate was reached in the last cycle. Hence, the probed depth corresponds to the entire thickness of the film.

The RBS measurements were performed at the tandem accelerator in Uppsala using 2.00 MeV He^+ ions. The amount of oxygen in the films was investigated for samples grown on polished pyrolytic graphite substrates. These substrates do not contribute to the background at energies above approximately 0.5 MeV, making it possible to detect even very small amounts of oxygen in the samples. Moreover, it is also possible to distinguish between oxygen adsorbed at the surface, absorbed in the film and adsorbed at the film–substrate interface. The measured RBS data were analysed using the RUMP software[4] [19]. Further details about the RBS method can be found elsewhere; see for example [20].

The changes in optical properties upon hydrogen loading were investigated using an Ocean Optics S2000 spectrometer. The measurements were performed *ex situ*, in a transmission set-up with the wavelength ranging from 220 to 1100 nm. A tungsten–halogen light source (HL-2000) was used for photon wavelengths between 360 and 1100 nm (3.44–1.13 eV). For wavelengths below 360 nm, i.e. the interval 220–359 nm (5.64–3.45 eV), a variable pulsed xenon lamp was used (Ocean Optics PX-2).

The ^{15}N method was used for performing the depth profiling [21] of hydrogen in the samples, at the tandem accelerator in Uppsala. The technique is based on the $^1H(^{15}N, \alpha\gamma)^{12}C$ nuclear resonance reaction, in which the hydrogen depth profile as well as the total amount of hydrogen is determined. When performing hydrogen profiling, the sample is bombarded

[4] http://www.genplot.com

by ^{15}N ions with an energy equal to or above the resonance energy (6.385 MeV). The energy was changed in steps of 0.025 MeV during all measurements. Upon penetration, the ions lose energy and at a depth at which the ions have the resonance energy, the probability for the reaction is greatly enhanced. The depth resolution is about 1 nm, close to the surface, but degrades with increasing depth, due to energy straggle. The detection limit is typically some atomic ppm and the precision is determined by the counting statistics. The accuracy is governed by the calibration standard and the accuracy in the stopping powers. The samples were cooled to 77 K using liquid nitrogen to prevent any desorption of hydrogen during the measurements.

3. Results and discussion

3.1. Mg–Ni multilayers: annealing effects and hydrogen loading

Annealing can be used to homogenize the distribution in multilayered films. However, the required annealing time and temperatures are strongly linked to the thickness of the layers and also the nature of the elements.

The annealing was performed on samples with the bilayer thickness of 2 nm. The resistivity was monitored during the annealing procedure. It increased close to linearly in the temperature interval 298–355 K and in the range between 355 and 390 the change levelled out. At a temperature of approximately 393 K, a significant decrease in the resistivity was observed. At 440 K the rapid resistivity decrement comes to an end and only the expected linear increase was observed as the temperature was increased further. While cooling down, from 623 to 298 K, a linear decrease of the resistivity is observed indicating irreversible changes in the films. Upon additional heat treatment, the resistivity changed within this temperature interval (298–623 K). Judging from the resistivity measurements, we can conclude that the alloying process is fully completed (between 393 and 440 K) after the first cycle. It is to be noted that the same irreversible changes occurred irrespectively of the Mg–Ni ratio. To investigate the effect of the heat treatment and the irreversible changes in more detail, x-ray diffraction measurements were performed on one of the samples before and after heat treatment.

High angle XRD measurements from the as grown samples, as illustrated in figure 1, are consistent with nanocrystalline structures. Only a broad and faint Mg(002) peak at a 2θ equal to 34.39° is observed. Upon annealing—see figure 1—the Mg(002) peak vanishes and new Bragg peaks corresponding to Mg_2Ni and Mg_6Pd appear. The XRD pattern in figure 1 originates from a Ni rich position of the sample which gives a plausible explanation for the disappearance of the Mg(002) peak since most of the Mg is forming Mg_2Ni and Mg_6Pd. However, the x-ray diffraction measurements do not give any information on the depth distribution of these phases nor the relative quantity. Amorphous or nanocrystalline inclusions of the pure elements within the film have therefore to be considered in this context. The presence of the Mg_6Pd peak indicates that either Ni is diffusing towards the substrate (recall that the layer closest to the Pd cap is Ni) or Mg is diffusing towards the surface, upon annealing. Thermodynamic calculations support these observations, the total energy is reduced by segregation of Mg to the surface [22]. Mg readily forms Mg_6Pd when Pd is present. This process degrades the protective Pd layer. Furthermore, any Mg present at the surface will react with oxygen forming a passivating MgO layer. Here it should also be pointed out that an attempt at annealing in hydrogen atmosphere (5×10^{-2} bar) was performed and that the result from this experiment completely reflects the previously described and coming results.

The heat treated samples were further investigated using both XPS depth profiling and RBS. In figure 2 typical results from the XPS measurements are shown. The XPS electronic

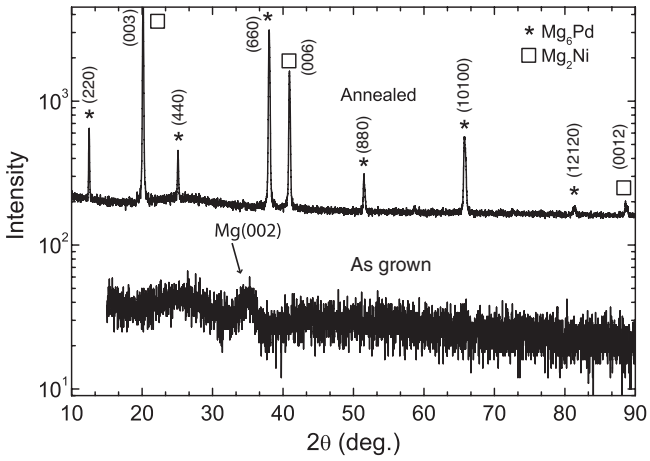

Figure 1. XRD patterns of a multilayered Mg–Ni thin film before and after annealing. The multilayer composition of the as grown film was 1.5 nm Mg and 0.5 nm Ni with 50 repetitions giving a total film thickness of 100 nm.

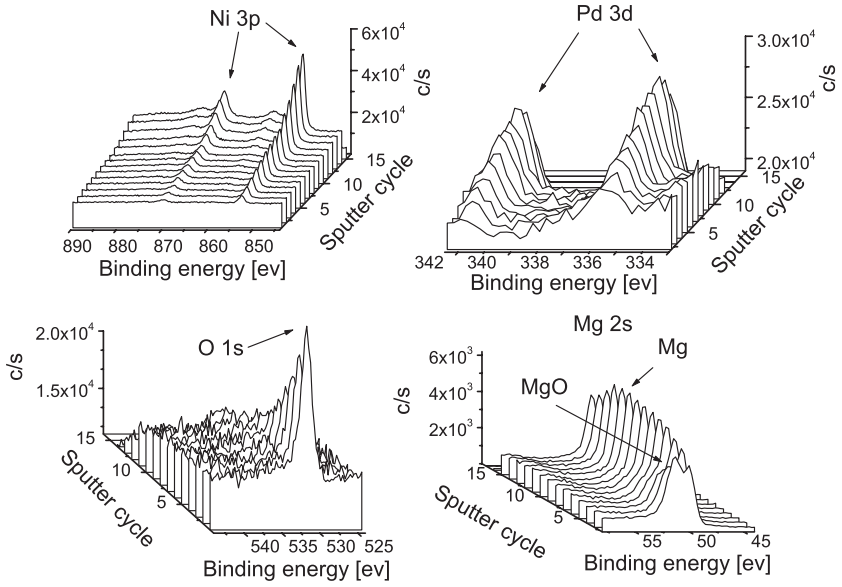

Figure 2. XPS depth profiles of the different elements present in the film after annealing.

levels used were Mg 2s, Ni 2p, O 1s and Pd 3d, qualitatively illustrating the elemental distributions as well as the oxidation states. The resolution of the Pd 3d peaks is reduced due to the emittance of Mg Auger electrons. The shape and the position of the Mg 2s and Ni 2p peaks agree with tabulated values for metallic Mg and Ni, respectively [23]. For Mg 2s (49.9 eV) the peak is shifted +1.5 eV due to the formation of MgO. This outermost surface layer disappears after nine sputter cycles (about 1 min), which corresponds to a thickness of about 10 nm. This feature is also confirmed by the simultaneous reduction of the O 1s peak. Hence, we can conclude that the thickness of the MgO corresponds approximately to 10 nm. The Mg

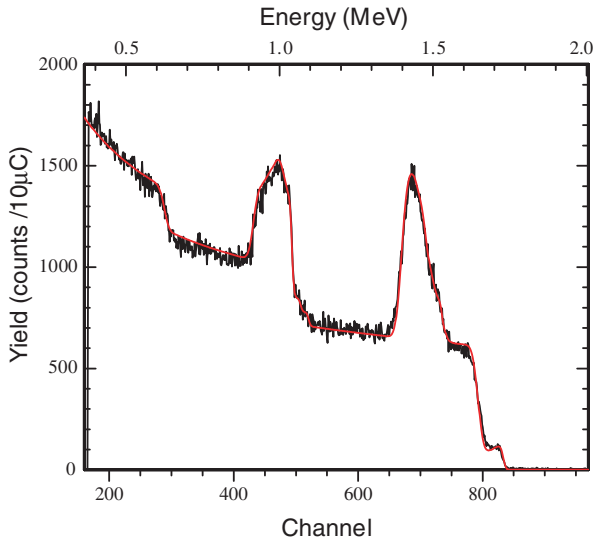

Figure 3. Results of the RBS measurements on the film after annealing. The curve represents the result of the reconstructed signal.

Table 1. Results of the RUMP modelling of the RBS measurements expressed as atoms per cm^2. Layer 1 represents the upper part of the film and 5 the near substrate region. The typical error on the elemental density is 2×10^{15} atoms cm^{-2}.

	Elemental density (10^{15} atoms cm^{-2})		
Layer	Pd	Mg	Ni
1	4	279	18
2	3	267	30
3	3	222	75
4	—	143	77
5	—	186	104

composition is approximately constant, as determined by the depth profile. From the position of the two Ni 2p peaks it can be concluded that Ni atoms are largely in the metallic state, in good agreement with earlier studies on bulk Mg–Ni alloys [24]. Moreover, the Ni atoms diffuse towards the substrate–film interface. No formation of Ni oxide was observed. The heat of formation is -602 kJ mol^{-1} for MgO and -241 kJ mol^{-1} for NiO. Thus the formation of MgO is thermodynamically more favourable [25]. The two peaks of Pd 3d (336.3 and 341.6 eV) are found to be shifted by +1.5 eV as compared to the tabulated value of Pd [23]. The origin of this energy shift can be explained by the formation of Mg_6Pd, also identified in the XRD patterns. As previously mentioned, measurements were made at a total of 16 points, of which one is illustrated in figure 2. The shape and distribution of the remaining 15 points resemble those presented here, although the intensities of the individual peaks are somewhat different due to the changes in the composition. As illustrated in figure 3, the RBS measurements confirm this picture and in table 1 the results from the modelling of the RBS data are presented. Due to the overlap of the signals from the substrate and oxygen in the films, it is not possible to

determine the oxygen content in the films on the glass substrates. The modelling of the RBS data using the RUMP software package is based on a five-layer model of the film. The results from the XPS and RBS measurements are in good agreement concerning the depth distribution of the elements; moreover, the RBS measurements also confirmed the thickness of the films as determined by x-ray reflectivity. In addition, the results from the XPS and RBS measurements are in agreement with earlier studies. Stefanov [26, 27] reported that Mg segregates to the surface in several $Mg_{1-x}Ni_x$ alloy films ($x = 0.5$–0.96) at temperatures of 500 K or higher and that MgO forms at the surface. This was also confirmed by Richardson *et al* [13] who annealed thin Mg rich Ni–Mg films in dry nitrogen up to 398 K.

To summarize the effect of the annealing treatment of Pd capped Mg–Ni multilayered thin films, we have shown that it results in the migration of Mg towards the surface of the films. As determined from the *in situ* probe resistivity measurements, this process becomes evident at a temperature of approximately 390 K. In contact with the Pd capping layer some of the Mg forms Mg_6Pd, 'transferring' Pd downwards into the film. After heat treatment the uppermost layers of the films consist almost exclusively of Mg. Any oxygen containing impurities will inevitably react with Mg under the formation of a passivating MgO layer, hindering any hydrogen uptake. From all the results from the alloying experiment taken together, it can be concluded that it is not feasible, even at moderate temperatures, to create Mg–Ni alloys through heat treatment of multilayered thin films under the conditions described.

3.2. Mg–Ni multilayers: monolayer by monolayer growth, hydrogen loading and optical properties

As discussed above, the use of annealing of multilayered films to form an alloy is hampered by the reaction with the capping layer, as well as the formation of Mg oxides in the near surface region. To remedy this, we decreased the thickness of the individual layers, down to the monolayer and sub-monolayer range. In growing these thin layers, an alloy is formed during the growth of the samples and consequently no annealing is needed for homogenization.

Because we grow one of the constituents (always Ni) as a wedge, a wide composition range is accessible on the same substrate. The configuration of the wedge samples is schematically illustrated in the upper panel of figure 4. The x-ray reflectivity measurements exhibited no multilayer peaks, consistently with the absence of chemical modulation. Moreover, it is possible to determine the changes in the composition arising from the wedge growth. The lower panel of figure 4 shows typical changes in the composition of the as grown films, as determined by means of RBS. The high angle XRD patterns from the as grown wedge multilayered films, not shown here, are consistent with amorphous or nanocrystalline samples.

When discussing the absorption energies, as well as the optical properties, the chemical purity of the samples is crucial. Mg reacts readily with oxygen, forming MgO. One reference sample was therefore grown on a substrate of polished graphite, in order to determine the typical oxygen concentrations in the samples. The results from RBS measurements are illustrated in figure 5. The interior of the film appears to be oxygen free. The small amount of oxygen, detected at an energy of approximately 0.7 MeV, originates from oxygen containing species adsorbed on the surface of the film. The as determined elemental densities of oxygen were 5 and 12×10^{15} atoms cm^{-2}, at the surface and at the film–substrate interface, respectively.

During the hydrogen loading the samples began to switch from the reflecting metallic state towards transparency. This transformation occurred gradually over the samples and was initially observed in the Ni rich part. The samples were typically loaded for a maximum duration of 60 h and exhibited a pale yellowish colour in the Mg rich parts and, as the Ni content increased, the colour gradually turned to a dark brownish shade. The nature of the

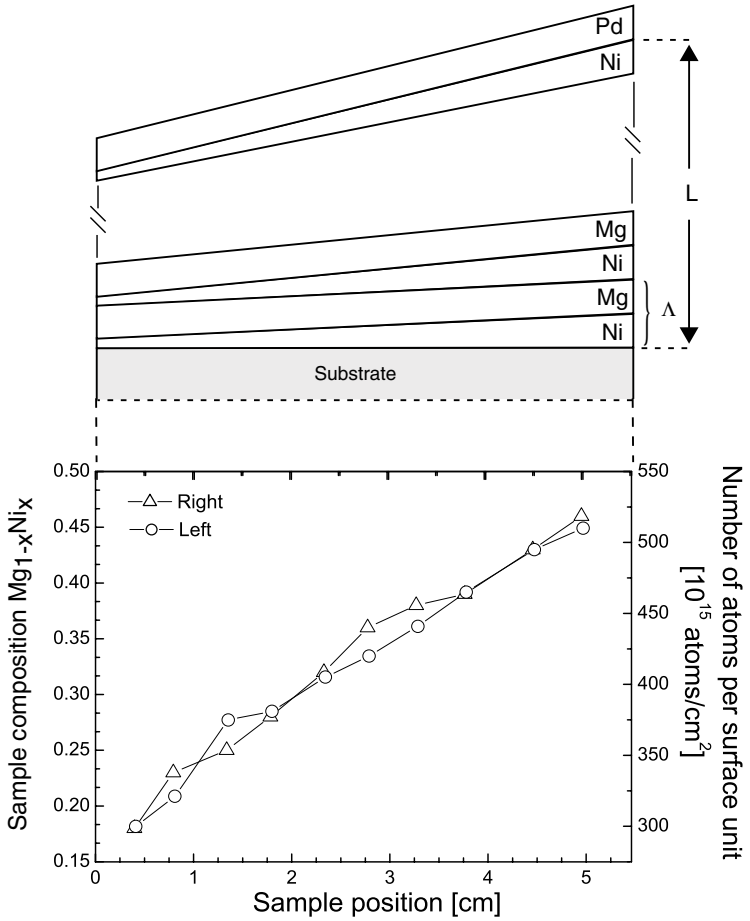

Figure 4. The upper panel schematically illustrates the wedge film design. The lower panel shows the sample composition ($Mg_{1-x}Ni_x$) and the number of atoms per surface unit as determined by RBS measurements.

colour change of the samples, however, indicates that Mg_2NiH_x has formed. In addition, the transparency in the region of the lowest Ni content indicates that MgH_2 has formed. The absence of the diffraction lines characteristic of these compounds in the diffractogram is most likely due to nanocrystallinity and the small amounts of material present. Recall that the total film thickness is only 70 nm, in the thickest part.

The results from the NRA hydrogen depth profiling measurements are presented in figures 6 and 7. Depth profiling was performed at a total of eight positions on the sample. For clarity, only five positions corresponding to a sample compositions of $Mg_{1-x}Ni_x$ where x is equal to 0.17, 0.27, 0.34, 0.41 and 0.43 are presented in figure 6. For all compositions, the hydrogen distribution can be described as being homogeneous throughout the sample, although one might discern a tendency towards a lower hydrogen concentration closer to the surface for the two highest Ni concentrations. Judging from these results it can be concluded that there is a homogeneous distribution of sites with similar absorption energies throughout the film. The maximum energy needed for the ^{15}N ions to reach the substrate is changing as the different regions in the films have different thicknesses. In figure 7 the atomic ratio between hydrogen

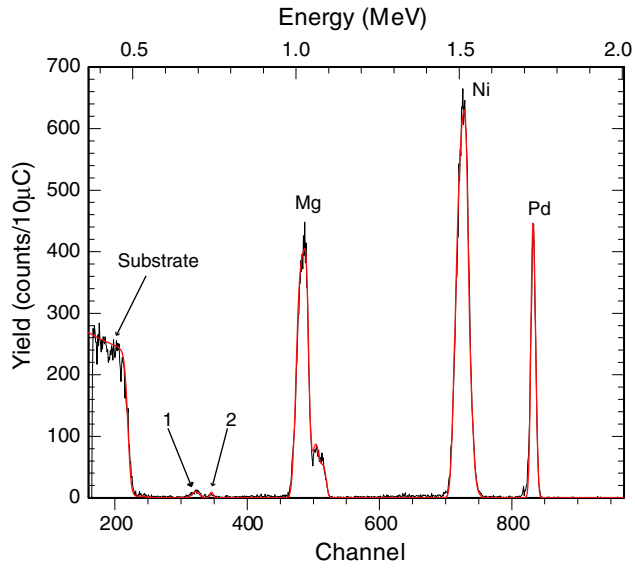

Figure 5. RBS results for a wedge multilayer grown on a polished graphite substrate. Indices 1 and 2 indicate the oxygen at the surface and the substrate–film interface respectively. The curve represents the result of the reconstructed signal.

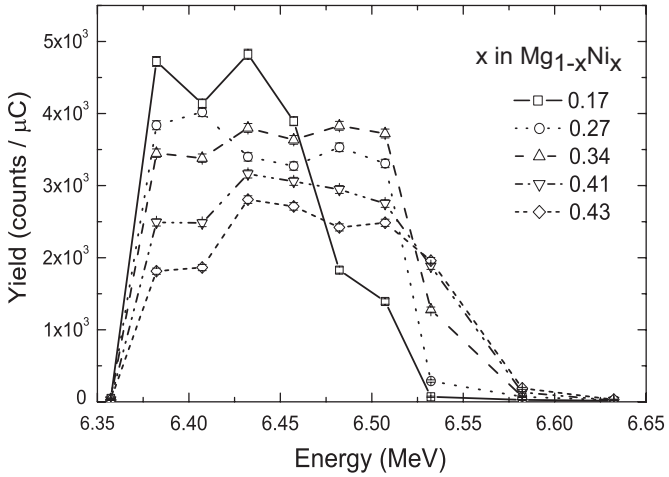

Figure 6. Hydrogen depth profiles at five different ratios of Ni.

and metal (H/M) as a function of Ni content in the film is illustrated as well as the expected values for MgH_2 and Mg_2NiH_4. The hydrogen concentration decreases almost linearly with increasing Ni content and the maximum hydrogen uptake capacity for a Ni atomic ratio of 0.33 (Mg_2Ni) is close to the theoretical maximum value of 1.33 H/M of Mg_2NiH_4 [3].

The effective optical band gap, denoted as E_g^{eff}, was determined using a linear extrapolation formalism. The slope of the line at the inflection point, after the transmission edge, is linearly extrapolated to zero transmission and is deduced to be E_g^{eff}. In addition, E_g was determined using the Lambert–Beer law, $T(\omega) = T_0 \exp(-\alpha(\omega)d)$, where α is the absorption coefficient, d the film thickness and T_0 invokes the transmission of the Pd capping layer and

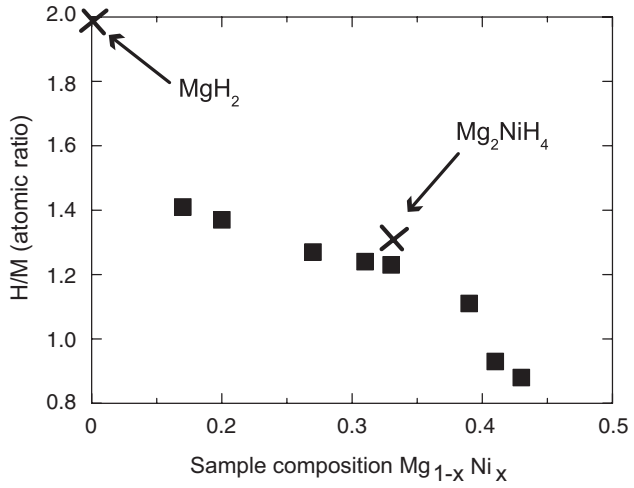

Figure 7. Maximum hydrogen uptake capacity expressed as H/M. For comparison, the values for MgH_2 and Mg_2NiH_4 are included.

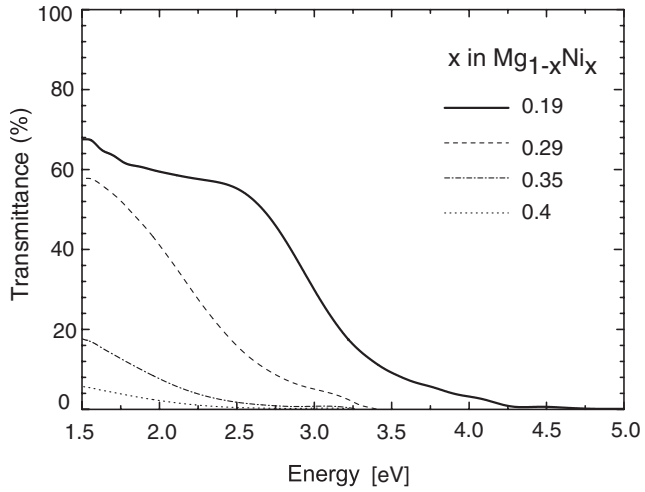

Figure 8. The change in transmittance for a wedged multilayered film loaded with hydrogen to a maximum pressure of 1 bar.

the substrate. Figure 8 illustrates the transmission curves at four different positions on the sample while figure 9 shows the corresponding effective optical band gap as determined by the linear extrapolation method as a function of the sample composition. The maximum transmittance clearly differs at different positions on the sample. The maximum transmittance decreased systematically with increasing Ni content. This feature arises from scattering and absorption processes linked to unpaired Ni electrons. As seen in figure 8, the transmission curves does not exhibit a regular single-component asymptotic behaviour while approaching zero transmittance. The tail, best illustrated in the curve for the Mg rich region, indicates that the transmission is dependent upon more than one component. In a first approximation, the total band gap ($E^{\mathrm{eff}}_{\mathrm{g,tot}}$) can be estimated as a weighted summation of the fractional components

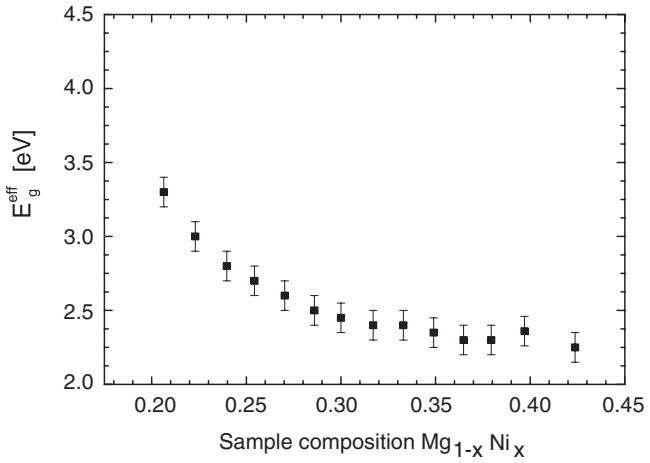

Figure 9. The change in optical band gap for a wedged multilayered film loaded with hydrogen to a maximum pressure of 1 bar.

of the band gap for MgH_2 and Mg_2NiH_4. If the Lambert–Beer law is used to derive the optical band gap, this feature is to a large extent neglected while the linear extrapolation formalism to some extent also includes these effects. The values for E_g as a function of the Ni content as determined from the Lambert–Beer approach are approximately 0.6–0.8 eV lower than those determined from linear extrapolation method. This gives a band gap of approximately 1.6–1.8 eV for Mg_2NiH_4 which is in agreement with previous reported results from for example Isidorsson, Yoshimura and Meyers [11, 12, 15]. In addition E_g for MgH_2 has been reported by Isidorsson *et al* to be between 5.61 and 5.67 eV [10]. The estimated value for Mg_2NiH_4 in this study, E_g^{eff} equal to 2.4 eV, therefore has to be considered to be somewhat overestimated since it is $E_{g,tot}^{eff}$ that has been measured and not solely E_g^{eff} for Mg_2NiH_4. From the purity of the films, with respect to oxygen content (as determined by means of RBS)—recall figure 5—we can conclude that MgO, with a band gap of 7.77 eV [16], is not affecting the deduced value of E_g^{eff}.

The curve in figure 9 can be considered as composed of two linear regions, $0.15 \leqslant x < 0.3$ and $x \geqslant 0.3$. The band gap in the first region decreases when the Ni concentration increases. This feature originates from the contributions of both MgH_2 and Mg_2NiH_4 to the effective band gap. The amount of Ni in this part of the sample is not sufficient on its own to form the Mg_2Ni. Furthermore, if the curve in figure 9 is extrapolated to Ni/Mg equal to 0 (pure MgH_x), E_g^{eff} can be deduced to be approximately 4 eV. This value is significantly lower than the one determined by Isidorsson *et al* [10], 5.61–5.67 eV. In the second region, E_g^{eff} is equal to approximately 2.4 eV and does not depend on the excess of Ni. All the Mg is expected to have alloyed with Ni forming Mg_2Ni. Hence no MgH_2 can influence the level of the band gap. Hence the excess of Ni results in a lowering of the transmission but does not affect the overall band gap.

4. Summary and conclusions

Thin films of Mg–Ni have been grown by DC magnetron sputtering. Mg starts to diffuse and migrates towards the surface upon annealing, even at moderate temperatures (above 393 K), as demonstrated by XRD, XPS and RBS studies. The Pd capping layer degrades while forming

Mg_6Pd and a surface layer of MgO, and no hydrogen uptake could be observed. Thereby it can be concluded that formation of hydrogen absorbing alloys by heat treatment of Mg–Ni thin films at temperatures above 393 K is not plausible.

Wedged multilayers with individual layer thicknesses on the monolayer scale allow us to access a wide range of compositions on one and the same sample. Furthermore, these thin films prove to absorb hydrogen at 298 K. Hydrogen depth profiling measurements revealed that the absorbed hydrogen is evenly distributed in the sample and that the hydrogen uptake capacity decreases almost linearly with increasing Ni content. The uptake capacity for a Ni ratio of 0.33, which corresponds to Mg_2Ni, is deduced to be close to the theoretical maximum capacity of H/M = 1.33 (Mg_2NiH_4). During the absorption process the samples undergo a transformation from a reflecting metallic to a coloured pale yellowish to brownish (Mg rich to Ni rich) transparent semiconducting state corresponding to a change in the effective optical band gap of 3.6 (Ni poor) to 2.4 (Ni rich) eV. The decrease of the effective optical band gap goes together with a decrease of the maximum transmittance which is related to the presence of free conduction electrons originating from pure Mg and Ni. The change in band gap as a function of Ni concentration appears to be composed of two regions. While the Ni concentration is increased, the band gap decreases approximately linearly until the composition of $Mg_{0.7}Ni_{0.3}$ is reached. For higher Ni concentrations the effective band gap is constant at about 2.4 eV. The presence of oxygen in the film, as determined from RBS measurements, was below the detection limit and is too small to influence the band gap determined. The extrapolated value of E_g^{eff} for MgH_x (3.6 eV) is far from the values of MgH_2 (5.7 eV) as determined by Isidorsson *et al* [10].

Acknowledgments

This project was financially supported by the Swedish Energy Administration and the Swedish Research Council. The authors would also like to thank Jonas Åström and Gösta Widman from the tandem laboratory at Uppsala University for running the accelerator. Finally Ola Wilhelmsson is thanked for help with the XPS measurements.

References

[1] Stampfer J F Jr, Holley C E Jr and Suttle J F 1960 *J. Am. Chem. Soc.* **82** 3504
[2] Stander C M 1977 *J. Inorg. Nucl. Chem.* **39** 221
[3] Reilly J J and Wiswall R H 1968 *Inorg. Chem.* **7** 2254
[4] Akiba E 1999 *Curr. Opin. Solid State Mater. Sci.* **4** 267
[5] Orimo S and Fuji H 2001 *Appl. Phys.* A **72** 167
[6] Nomura K, Akiba E and Ono S 1981 *J. Inst. Energy* **6** 295
[7] Holtz R and Imam M 1997 *J. Mater. Sci.* **32** 2267
[8] Holtz R, Imam M and Meyn D A 1995 *Synthesis/Processing of Light Weight Materials* (Warrendale, PA: The Minerals, Metals and Materials Society) p 339
[9] Chen J, Yang H B, Xia Y-Y, Kuriyama N, Xu Q and Sakai T 2002 *Chem. Mater.* **14** 2384
[10] Isidorsson J, Giebels I A M E, Arwin H and Griessen R 2003 *Phys. Rev.* B **68** 115112
[11] Isidorsson J, Giebels I A M E, Griessen R and Di-Vece M 2001 *Appl. Phys. Lett.* **80** 2305
[12] Yoshimura K, Yamada Y and Okada M 2002 *Appl. Phys. Lett.* **91** 4709
[13] Richardson T J, Slack J L, Kostecki R and Rubin M D 2001 *Appl. Phys. Lett.* **78** 3047
[14] Richardson T J, Wang L-W, Farangis B and Rubin M D 2002 *Appl. Phys. Lett.* **80** 1349
[15] Meyers W R, Wang L-W, Richardson T J and Rubin M D 2002 *J. Appl. Phys.* **91** 4879
[16] Sheik-Bahae M, Hutchings D C, Hagan D J and Stryland E W V 1991 *IEEE J. Quantum Electron.* **27** 1296
[17] Pick M A, Davenport J W, Stronging M and Dienes G J 1979 *Phys. Rev. Lett.* **43** 286
[18] Stillesjö F, Olafsson S, Isberg P and Hjörvarsson B 1995 *J. Phys.: Condens. Matter* **7** 8139

[19] Doolittle L R 1985 *Nucl. Instrum. Methods Phys. Res.* B **15** 227
[20] Bird J R and Williams J S 1989 *Ion Beams for Material Analysis* (Australia: Academic)
[21] Lanford W, Trautvetter H, Ziegler J and Keller J 1976 *Appl. Phys. Lett.* **28** 566
[22] Abrikosov I 2004 private communication
[23] Wagner C D, Riggs W M, Davis L E, Moulder J F and Muilenberg G E 1979 *Handbook of X-Ray Photoelectron Spectroscopy* 2nd edn, ed C D Wagner, W M Riggs, L E Davis, J F Moulder and G E Muilenberg (Eden Prairie, MN: Perkin-Elmer Corporation)
[24] Schlapbach L, Schaltiel D and Oelhafen P 1979 *Mater. Res. Bull.* **14** 1235
[25] Selvam P, Viswanathan B, Swamy C S and Srinivasan V 1990 *J. Less-Common Met.* **163** 89
[26] Stefanov P 1995 *Vacuum* **9** 1107
[27] Stefanov P 1997 *Appl. Surf. Sci.* **108** 477